IOP Publishing Superconductor Science and Technology
Supercond. Sci. Technol. 31 (2018) 115003 (9pp) https://doi.org/10.1088/1361-6668/aade1d

A high-temperature superconductor under applied strain: vortex dynamics and critical current density

Vladimir A Kashurnikov, Anastasiia N Maksimova, Anna N Moroz[1] and Igor A Rudnev

National Research Nuclear University MEPhI (Moscow Engineering Physics Institute), 115409, Kashirskoe shosse, 31, Moscow, Russia

E-mail: ANMoroz@mephi.ru

Received 21 May 2018, revised 14 August 2018
Accepted for publication 31 August 2018
Published 20 September 2018

Abstract

By using the Monte Carlo method, a numerical study has been conducted to investigate the influence of strain on the critical current density and voltage–current characteristics of a high-temperature superconductor. It has been shown that if a sample is strained, the critical current density and the slope of the *E–J* curve decrease. Staircase *E–J* curves of strained samples corresponding to alternating states of vortex freezing and defreezing have been discovered. Vortex dynamics has been demonstrated for different degrees of strain. A possibility of almost unhindered movement of vortices towards the center of the sample along the occurring areas of stress has been shown for heavily strained samples.

Keywords: HTSC, vortex dynamics, bending strain, Monte Carlo simulation, critical current density

(Some figures may appear in colour only in the online journal)

1. Introduction

The development of high-temperature superconductor (HTSC) manufacturing technologies has led to the use of HTSC in various power applications such as cables, engines, windmills, magnets, etc. However, the brittleness of HTSC materials is a serious problem. During fabrication and use of HTSC-based tapes and wires, their superconducting layers experience different mechanical loads capable of degrading the transport characteristics of HTSC to the point of complete loss of superconductivity. Bending strains occurring during winding of tapes or wires into magnet coils [1–12] are of special importance. On the other hand, strained samples may exhibit higher critical current densities due to associated pinning [13–15].

A great amount of experimental and theoretical research has been dedicated to a comprehensive study of the influence of mechanical strains on the transport characteristics of $YBa_2Cu_3O_{7-x}$ (YBCO) coated conductors [1–6] and Bi–Sr–Ca–Cu–O (BSCCO) tapes and wires [7–12]. There have been various studies of the effect of different substrate materials and stabilizing buffer layers [1–4] on the critical current I_c stability of YBCO coated conductors (CC), as well as the effect of reversibility of critical current degradation [5]. There have even been attempts to visualize the distribution of critical current density j_c of CC under strain by using the scanning Hall magnetometry [6]. The influence of bending and torsion strains on the critical current of $Bi_2Sr_2Ca_2Cu_3O_{10+x}$ (Bi-2223) tapes have been thoroughly studied in [7]. Half-empirical models of the I_c dependence on bending strain of Bi-2223 tapes have been reported in [8–10]. Tensile strains and the mechanical strain reversibility effect have also been studied in Bi-2223 samples [11, 12]. All the above-mentioned investigations have shown that applying strain leads to I_c degradation. The pictures obtained via scanning electron microscopy in [3, 4, 9, 12] demonstrate cracking of both YBCO and BSCCO samples which is suggested to be the major reason behind I_c degradation.

As is well known, the transport and magnetic characteristics of HTSC are in many respects determined by the vortex pinning and dynamics [13–24]. It is difficult to analytically solve the problem of vortex dynamics in HTSC. Therefore, to take into

[1] Author to whom any correspondence should be addressed.

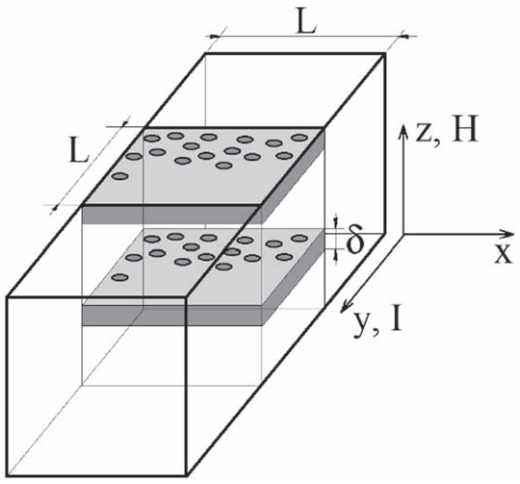

Figure 1. The geometry of calculations.

account all of the features of a vortex system and obtain accurate results, the continuous-space Monte Carlo method seems the most appropriate [16–24]. This method has already been successfully applied to study the influence of ferromagnetic nanoparticles, temperature, and the concentration and distribution of pinning centers, on the magnetization processes [16–19] and flow of transport current [20–23]. Phase states and dynamics of a vortex system have also been studied in all of the mentioned papers. To the best of our knowledge, the influence of strain directly on the vortex dynamics has not been considered so far. In the present paper, a Monte Carlo simulation has been applied for the first time to study the vortex system in model HTSC samples under various degrees of strain. Voltage–current characteristics of strained samples have been calculated as well. The influence of strain on the critical current density has been determined.

The paper is constructed in the following way: section 2 is dedicated to the description of the calculation model and the samples under study, section 3 shows the main results such as the dependencies of critical current density (3.1) and slope of the *E–J* curves (3.2) on strain, as well as a detailed investigation of the vortex lattice dynamics in a strained HTSC (3.3).

2. The model

The geometry of calculations is shown in figure 1. HTSCs are mostly highly anisotropic layered materials and can be simplistically described as a system of alternating superconducting planes of thickness δ. The external magnetic field H_0 is parallel to the z-axis. The transport current I flows along the y-axis. For the task in question, a 2D $L \times L$ strip of a superconducting layer located in the xy-plane with periodic boundary conditions along the y-axis was chosen. In the considered model, it is assumed that the superconducting layers make additive contributions to the properties of the system with high anisotropy (like BSCCO for example). For that reason, the results for a single layer can be considered as an averaged response from the whole HTSC. In addition to that, for real multifilamentary BSCCO tapes, the total response is averaged among the constituent filaments. However, even for low-anisotropy materials like YBCO, the two-dimensionality of calculations can be justified when the sample contains a significant amount of impurities and/or is strained so that the correlations between adjacent layers are low [23].

The thermodynamic Gibbs potential that takes into account all the interactions in a 2D system with an alternating number N of vortices is the following [19, 20, 23, 24]:

$$G = \sum_{i<j} U(r_{ij}) + \sum_{i,j} U_{\mathrm{pn}}(r_{ij}) + \sum_{i,j} U_{\mathrm{surf}}(|r_i - r_j^{(\mathrm{image})}|) + \sum_i U_{\mathrm{m}}(x_i) + N\varepsilon, \quad (1)$$

$$U(r_{ij}) = \delta\Phi_0{}^2/(8\pi^2\lambda^2)K_0(r_{ij}/\lambda), \quad (2)$$

$$U_{\mathrm{pn}}(r_{ij}) = -\alpha \exp(-r_{ij}/2\xi)/(1 + r_{ij}/\xi), \quad (3)$$

$$U_{\mathrm{surf}}(|r_i - r_j^{(\mathrm{image})}|) = -\delta\Phi_0{}^2/(16\pi^2\lambda^2)K_0(|r_i - r_j^{(\mathrm{image})}|/\lambda), \quad (4)$$

$$U_{\mathrm{m}}(x_i) = \delta\Phi_0/4\pi\{H_0[\cosh(x_i/\lambda)/\cosh(L/2\lambda) - 1] + H_I[-\sinh(x_i/\lambda)/\sinh(L/2\lambda) \pm 1]\}, \quad (5)$$

$$N\varepsilon = N\delta\Phi_0{}^2/(4\pi\lambda)^2(\ln(\lambda_0/\xi_0) + 0.52). \quad (6)$$

It consists of a sum of the interaction energies of vortices with each other (2), pinning sites (3), sample surface (4), magnetic field (the first term in (5)) and transport current (the second term in (5)). It also contains a sum of vortices' own energies (6). Here, r_{ij} is the distance between the vortex i and: another vortex (2), a pinning site (3) or a vortex image (4), j. r_i is the position vector of a vortex i, $r_j^{(\mathrm{image})}$ is the position vector of a vortex image j, x_i is the x-coordinate of a vortex i, λ is the magnetic field penetration depth, ξ is the coherence length, $\Phi_0 = 2.07 \times 10^{-7}$ Gs cm^2 is the magnetic flux quantum, α is the defect potential well depth, H_I is the magnetic field of the transport current, and K_0 is the Bessel function of imaginary argument. The values of λ and ξ share the same temperature dependence: $\lambda = \lambda_0[1 - (T/T_c)^{3.3}]^{-1/2}$, $\xi = \xi_0[1 - (T/T_c)^{3.3}]^{-1/2}$ where $\lambda_0 = \lambda(T = 0\,\mathrm{K})$, $\xi_0 = \xi(T = 0\,\mathrm{K})$, and T_c is the critical temperature. The form of the pinning potential in (3) does not affect the results when $\xi \ll \lambda$. It was chosen out of convenience the same as in [19, 22, 23].

When a transport current I flows through the sample, it creates an energy potential which leads to the appearance of vortices of different signs on opposing sides of the sample (along the x-axis). Henceforth, we shall denote a magnetic flux directed towards the positive z-axis (a counterclockwise circular current) as a vortex whereas a flux directed towards the negative z-axis shall be denoted as an antivortex (a clockwise circular current). According to the property of oppositely circulating currents, the interaction between a vortex and an antivortex is attractive. Correspondingly, vortices of the same sign repel each other. In our model, the expression in (5) is given as a work done by Lorentz force in moving a vortex from the edge of the sample to the center.

One of the main reasons behind transport characteristics degradation upon induced strain, according to [1, 3–9, 11, 12] is the cracking of the HTSC. Therefore, in this paper we shall introduce the concept of certain areas of stress inside the

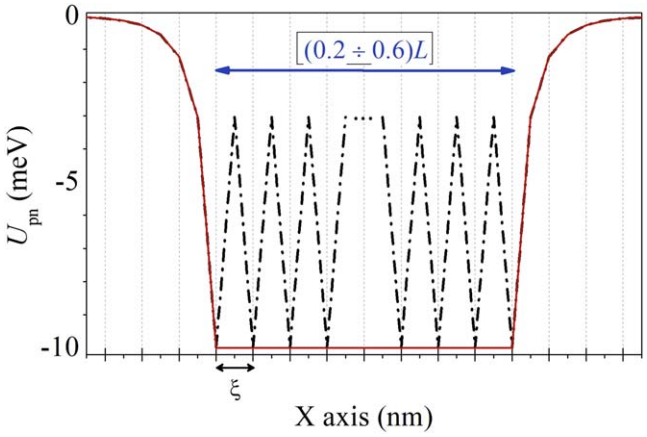

Figure 2. The energy potential of a crack. Because of the small distances between neighboring defects, each vortex interacts with the crack through the potential shown by the solid line. The potential well depth $\alpha = 0.01$ eV.

sample and call them 'cracks'. In our model, a crack shall be represented by a long chain along the x-axis made from a great number of closely spaced defects (the potential well of each defect is described by (3)). The distance between these individual defects is about the value of ξ. This concept is somewhat close to the normal core-size domain walls (or just a grain boundary) considered in [13]. Since the characteristic distance to which a vortex shifts per calculation step is about (1–10)ξ, a vortex occupying a crack does not feel its potential change as it moves along the crack. Thus, effectively each crack is an extended region of reduced superconducting properties as shown in figure 2.

The degree of strain shall be simulated by varying the quantity of such cracks in the sample. It should be noted that these cracks are not meant to represent the real microscopic cracks that appear in experiments and lead to a dramatic and irreversible decrease in j_c like in [1, 3–9, 11, 12], but rather the stress states of the crystal lattice that precede cracking and may not be visible by different visualization methods. In addition, the way our model cracks (or their conglomerates) affect the Abrikosov vortices is similar to that of the large-scale cracks. The direction of the cracks is chosen to be perpendicular to the current flow direction in correspondence with the way HTSC tapes and wires are bent in real superconducting magnet systems. The length of each crack is chosen randomly within the range from 0.2 to 0.6 of the sample length L. Such choice removed the need to elongate each crack when the strain is increased. The position of each crack along the x-axis is chosen randomly.

As has already been mentioned, the problem of the HTSC critical current tolerance to strains is relevant both for YBCO and BSCCO materials. In this paper, much the same as in our previous works [16–23] a Bi-2212 material has been chosen for investigation. Its parameters are the following: $\lambda = 180$ nm, $\xi = 2$ nm, $T_c = 84$ K, $\delta = 0.27$ nm. The number of pinning centers randomly distributed among the sample varied from 5000 to 45 000. The number of cracks varied from 0 to 1500. All calculations have been carried out using the continuous-space Monte Carlo method which has been explained in more detail in [19, 23].

3. Results and discussion

3.1. Influence of strain on the critical current density

In order to study the critical current density dependence on the degree of strain, series of voltage–current characteristics have been calculated for three samples with different values of two-dimensional density of randomly distributed defects n_d (2×10^{10}, 4×10^{10}, and 1.8×10^{11} cm^{-2}). The calculation of E–J curves was made possible by adding to the standard set of algorithm subprocesses (creation, destruction, and movement of a(n) (anti)vortex) a special subprocess of annihilating a vortex–antivortex pair. As has already been mentioned in section 2, when the transport current I flows through the superconductor, there are two kinds of vortices present on opposing sides of the sample. Driven by the Lorentz force, they move towards the sample center. If a vortex and an antivortex are separated by a relatively small distance ($\leqslant 9\xi$), the annihilation process takes place and the released energy turns into Joule heat. The total heat Q can be calculated by summarizing the contributions from all pair annihilations over a certain number of Monte Carlo steps. Given that $Q = \text{const} \cdot j \cdot E \cdot \Delta t$ and knowing the value of j at which the annihilations initiated (which is j_c by definition), we can derive the electric field E induced in the sample. Since there is no real time in our calculations, we need to normalize the result to experimental E–J curves, i.e. correlate j_c with the standard electric field criterion $E_c = 1\ \mu$V cm^{-1} used in most experiments. Thus, by calculating Q for each value of j and evaluating E, we obtain an E–J curve and determine the critical current density j_c by the mentioned electric field criterion (see [20, 23] for more details).

For each sample, the gradual increase in the degree of strain was modeled by adding new cracks to a sample. For each calculated series of E–J curves, a critical current density j_c dependence on the number of cracks N_c was obtained. All three dependencies are shown in figure 3. A clear gradual decrease in the critical current density with the increasing number of cracks can be seen for each curve. All three curves exhibit an oscillating behavior in the range of N_c from 90 to 360 which is shown in a close-up insert in figure 3.

Figure 4 shows the j_c dependencies on N_c normalized to the critical current density of an unstrained sample j_{c0}. The number of cracks can be approximately converted into real strain by evaluating the ratio of the area occupied by cracks to the total area of the sample. Normally, the strain is defined by the sample elongation divided by the initial length. However, considering the smallness of the sample length (5 μm), its elongation due to strain is negligible, so the computational volume stays the same and the number of cracks (or rather their linear density) simulates the strain. The sample area $S = 25\ \mu$m^2. The cracks have a width of approximately 2ξ and an average length of $0.4L$. Hence, for the case of $N_c = 30$ the strain will amount to $\propto$(0.96–1.2)%. The j_c/j_{c0}

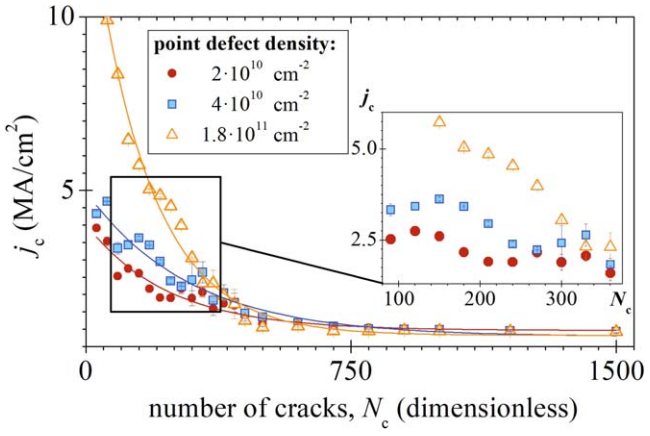

Figure 3. The critical current j_c dependencies on the number of cracks N_c for samples with different defect concentrations. The lines of corresponding colors show the fitted decay functions that most accurately describe the calculation points. The insert shows a scaled part of the dependence from 80 to 370 cracks to demonstrate the oscillating behavior of the calculated points.

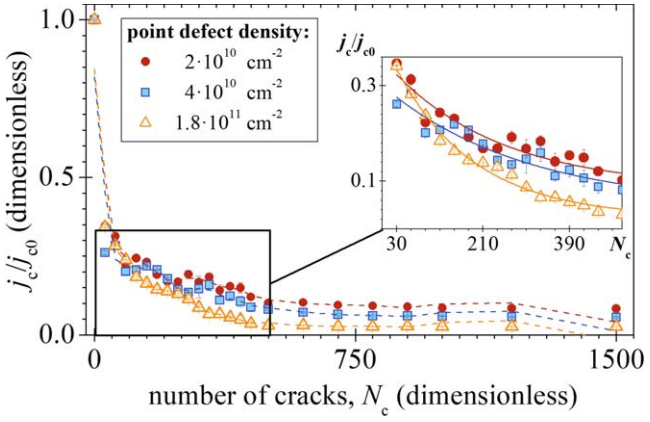

Figure 4. The normalized j_c/j_{c0} dependences on the number of cracks for different defect concentrations. A zoomed-in region of the dependence for j_c/j_{c0} from 0% to 36% is shown in the insert.

ratio for the mentioned number of cracks $N_c = 30$ can be determined as $\propto$(25–35)% from figure 4 (depending on different defect densities).

Similar critical current-bending strain dependences have been reported in papers [7, 10, 12]. In these papers, the normalized critical current was determined in Bi-2223 tapes at strains up to 1%, at liquid nitrogen temperatures and under self magnetic field of the transport current. The critical current I_c was determined by the same 1 μV cm^{-1} criterion as in our paper. The overall shapes of the reported dependencies are similar to those presented in figure 4. However, for the bending strain of 1%, the mentioned works report $I_c/I_{c0} = (50–70)\%$, whereas in our case, this value amounts to (25–35)% (given that the computational volume stays the same, $I_c/I_{c0} \approx j_c/j_{c0}$). The reason behind the difference may be that our calculations were carried out for the pure Bi-2212 material, whereas the samples in [7, 10, 12] were multifilamentary tapes that contained not only the superconductor itself but also a sheath of Ag and/or Ag alloy (with different

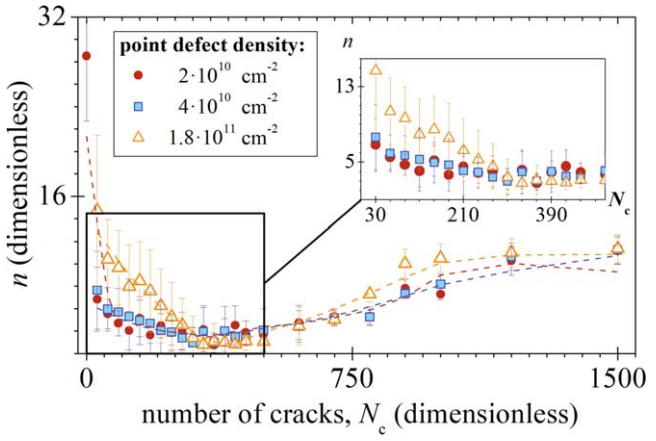

Figure 5. The calculated n-value dependences on the number of cracks for three defect concentrations. The part of the dependence in which n-value decays as expected from experiment is shown in the insert.

filament/Ag ratios) which can absorb some of the applied strain and prevent the material from premature cracking. In addition, in [7, 10, 12], the Bi-2223 material was considered, whereas in our model, Bi-2212 samples were considered. Although according to [25], Bi-2212 has similar mechanical properties to Bi-2223, the discrepancy between the studied materials may be another reason behind the difference in the obtained results. Thus, the results obtained in our work are in a qualitative agreement with the experimental data of [7, 10, 12].

3.2. Influence of strain on the n-value

The exponent of an E–J curve known as n-value is commonly used as a quality indicator for HTSC materials [26–29]. It is particularly relevant in designing magnets [26–28] and current limiters [29]. The n-value describes the sharpness of the superconducting transition and allows to evaluate the pinning force and determine the pinning mechanism in the material [28, 30, 31]. According to the Kim–Anderson model [31], greater n-values correspond to greater pinning potential. At such conditions, a phenomenon called flux creep occurs when only individual vortices are able to move through the sample. Smaller n-values correspond to weak pinning at which the so-called flux flow is observed, and the vortex lattice moves as a single whole.

Different experimental E_c criteria may strongly affect j_c in superconductors [32, 33]. However, in our work we kept E_c and the electric field range for the n-value definition identical for all samples. Hence, this problem does not affect the result of our work.

Figure 5 shows the calculated results for the n-value dependence on the number of cracks N_c. For each E–J curve, the n-values were determined in the electric field range from 0.1 to 4.0 μV cm^{-1} by using:

$$E = E_0(J/J_c)^n. \quad (7)$$

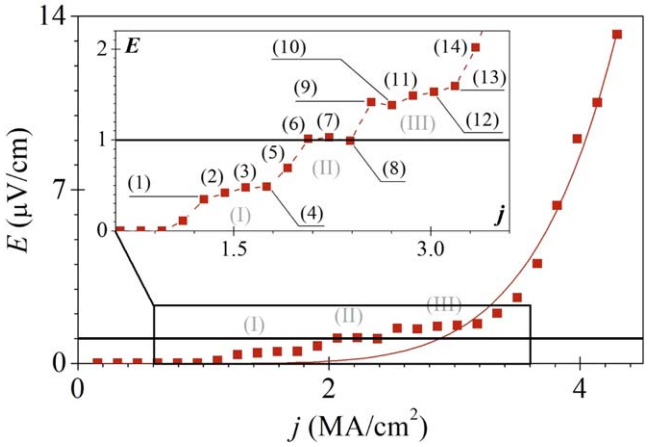

Figure 6. The *E–J* curve of a sample containing 300 cracks, $n_d = 4 \times 10^{10}$ cm^{-2}. The Roman numbers (I)–(III) denote the peculiar stairs on the curve. The insert shows them in more detail. The numbers (1)–(14) denote the points in which the vortex behavior was studied.

Figure 5 shows that upon increasing the level of strain, the *n*-value decays in agreement with the experiments [1, 7, 8, 25, 26]. The decay is particularly steep in the range of N_c from 0 to 100. Then, from $N_c = 300$ to 450, the *n*-value reaches a constant value of ∼(2–3) and starts to grow at $N_c \geqslant 500$. It should be noted that to our knowledge, the *n*-value-strain dependence has not been reported for strains exceeding (1–2)%, whereas our estimations suggest that the case of $N_c = 450$ corresponds to strain of ∝(14–15)% (the same as has been done for the case of $N_c = 30$ in section 3.1), which would lead to fracture in a real sample. Generally, upon degrading superconducting properties, the *n-value* should also decrease. Hence, in the range of $N_c = 450$–1500, the calculated *n*-value-strain dependence becomes unattainable in practice (figure 5). Thus, it represents the limit of applicability of our model. The results obtained within the mentioned range exceed the critical values of strain.

3.3. The dynamics of the vortex lattice of a strained HTSC

Upon calculating a series of *E–J* curves, we have observed some staircase peculiarities. Figure 6 shows one of the peculiar curves which was calculated for a sample with $N_c = 300$ and $n_d = 4 \times 10^{10}$ cm^{-2}. Each 'stair' of the *E–J* curve is indicated by a Roman numeral (I), (II) or (III). Additionally, figure 6 shows the zoomed-in part of the curve to demonstrate the stairs in more detail. Each point of the curve is numerated from (1) to (14). We have collected averaged vortex pictures for each of those points. The most illustrative are shown in figure 7. They correspond to the points (6) to (9) in figure 6. In each picture, vortices are depicted as blue circles (on the left of the sample) and antivortices are depicted as red triangles (on the right). The defects depicted as hollow squares and cracks depicted as dark solid horizontal lines are not to scale. The rectangular regions denoted by (a) and (b) in each figure indicate the zoomed-in areas shown in (6a)–(9a) and (6b)–(9b) in figure 7 for a more detailed study of the vortex dynamics.

In picture (6) of figure 7, the vortices are partially in motion which is demonstrated by the thick vortex and antivortex chains in the top right of the picture (at $y = 3.0$–4.5 μm). In this region, it is impossible to single out vortices as they form continuous lines due to their movement. This exhibits the flux-flow regime. It should be noted that this movement occurs predominantly along the cracks. In some regions, (for example, in the lower central part of picture (6)) the movement is weakened which allows determining the position of some vortices. The average distance between them is approximately 2λ.

In Figure 7(7), which is at the point of the *E–J* curve just at the defined E_c level, the vortex lattice stopped its movement almost completely, except for the region in the bottom right corner of the sample. Thus, the vortices froze allowing us to clearly distinguish practically each individual vortex. As a result, the number of vortex–antivortex pair annihilations was significantly reduced which led to a negligible change in the electric field ΔE as compared to that in picture (6) ($\Delta E = 0.02\ \mu$V cm^{-1} as opposed to $\Delta E = 0.32\ \mu$V cm^{-1} in figure 6). In Figure 7(8), the freezing of the vortex lattice intensified, and the electric field dropped below $E_c = 1\ \mu$V cm^{-1} ($\Delta E < 0$). In (9), which is at $E > E_c$, the vortices started moving again, which led to a sharp voltage jump on the *E–J* curve ($\Delta E = 0.43\ \mu$V cm^{-1}). As can be seen at point (10) in figure 6, the vortices froze again and remained frozen until point (13), from which they were gradually set in motion again with the increasing *j*. There was no more staircase behavior in the *E–J* curve. It should be noted that the vortices were never completely frozen at any stage of the *E–J* curves. This exhibits the flux creep regime with some vortices still hopping through the sample and annihilating with their counterparts. However, their number is negligible if compared to the total number of vortices in the sample, so the electric field is almost constant. This qualitatively agrees with the measurements of damping peak, indicating energy losses due to vortex movement, at the same temperature at which off-set of resistivity occurs in YBCO films [34]. Thus, this interchange between freezing and defreezing of the vortex system leads to the staircase *E–J* curves such as that shown in figure 6. All of the samples with the staircase *E–J* curves exhibited such vortex dynamics.

Since the cracks are regions with reduced superconducting properties that allow the vortices to lower their energy, each vortex finds it beneficial to move specifically along cracks. This can be illustrated by figure 8 where the averaged vortex pictures for four samples are shown with different degrees of strain. A transport current density $j = 2.5$ MA cm^{-2} flows through each sample. Figure 8(1)–(4) contain 0, 30, 60 and 300 cracks correspondingly. In figure 8(1), the vortices have entered the sample and got pinned by nearby point defects thus creating an energy barrier near the sample border that prevents the new vortices from entering the superconductor. The electric field *E* in the sample at this value of *j* is zero. However, in the presence of cracks, the situation changes. In figure 8(2), the vortices entering the sample near the cracks get a chance to move towards the center being pushed by the Lorentz force, and the electric

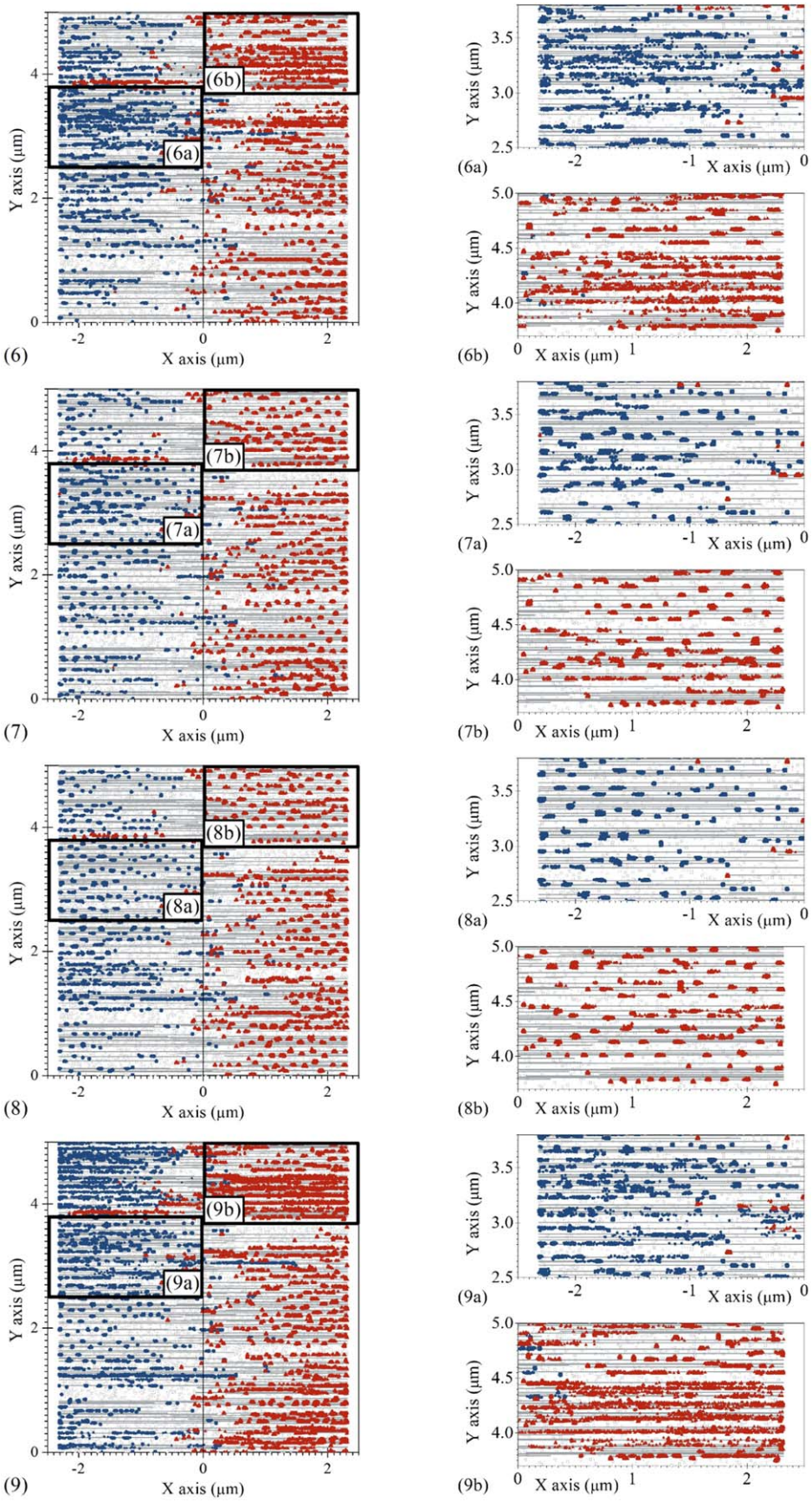

Figure 7. The averaged vortex configurations of a sample with defect density $n_d = 4 \times 10^{10}\,\mathrm{cm}^{-2}$ containing 300 cracks, obtained for the points (6)–(9) from step (II) of the E–J curve shown in figure 6.

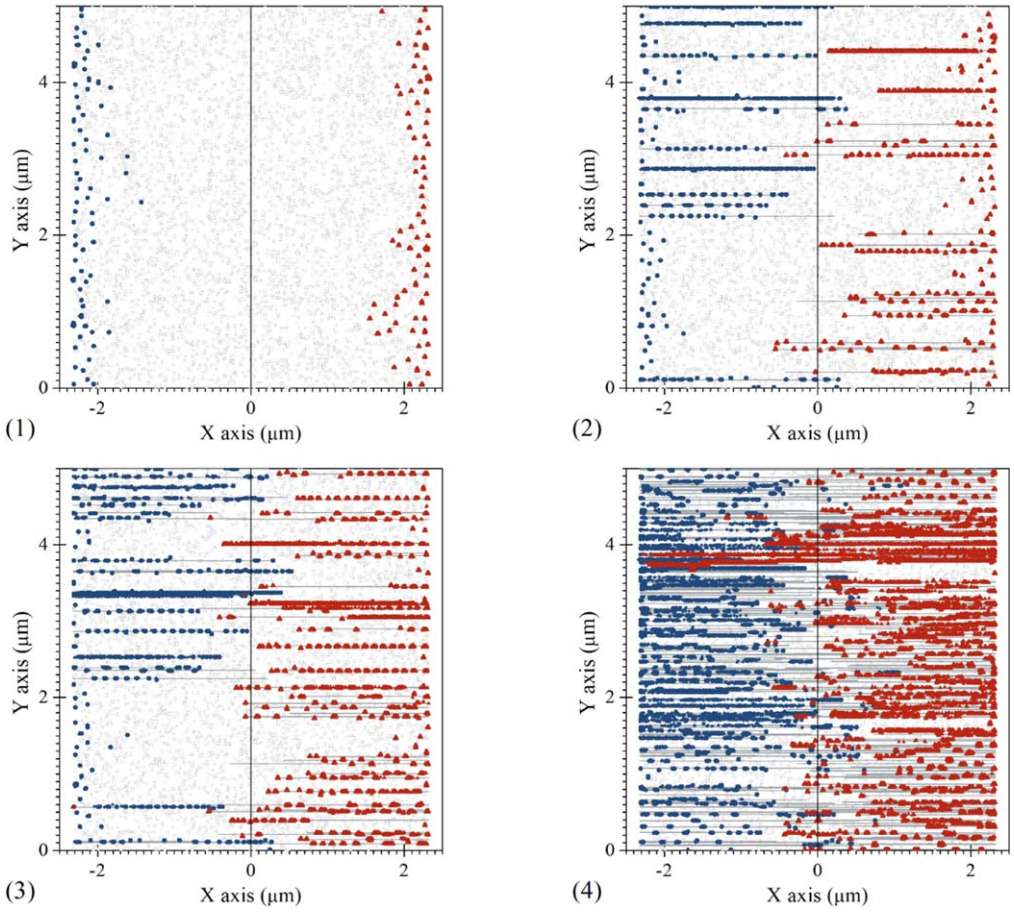

Figure 8. The averaged vortex configurations of samples with different numbers of cracks: 0 (1), 30 (2), 60 (3), and 300 (4). A current $j = 2.5\,\mathrm{MA\,cm^{-2}}$ flows through each sample. The point defect density $n_\mathrm{d} = 4 \times 10^{10}\,\mathrm{cm^{-2}}$.

field begins to rise much sooner than in the unstrained sample. As the degree of strain increases, so does the number of cracks, a larger number of vortices is able to reach the sample center. This is demonstrated in figures 8(3) and (4). As a result, the critical current density drops. It should also be noted that when the number of cracks is small (figures 8(2) and (3)), some vortices have the possibility to get pinned by defects and not take part in the overall movement of the system. If N_c is large (as in figure 8(4)), all vortex movements occur exclusively along the cracks so that pinning in the sample is suppressed.

As has been shown in figure 3, the $j_\mathrm{c}(N_\mathrm{c})$ dependences demonstrate oscillations for ($90 \leqslant N_\mathrm{c} \leqslant 360$). The minor j_c enhancements can also be explained by the occurrence of stairs in the *E–J* curves. Figure 9 shows the voltage–current characteristics of samples with point defect density of $4 \times 10^{10}\,\mathrm{cm^{-2}}$ and containing different numbers of cracks from 90 to 300. The interchanging freezing and defreezing of vortices have led to the case when, for example, the *E–J* curve for $N_\mathrm{c} = 120$, crossed the $E_\mathrm{c} = 1\ \mu\mathrm{V\,cm^{-1}}$ threshold at a much higher value of j than the one for $N_\mathrm{c} = 90$. This is in spite of the fact that it started to show nonzero electric field at smaller current densities (figure 9). In the sample with 120 cracks, at $j \sim 2.0\,\mathrm{MA\,cm^{-2}}$ the vortices froze and remained frozen until the current density reached $\sim$2.7 $\mathrm{MA\,cm^{-2}}$. The sample with 90 cracks also exhibited frozen vortices at $j \sim 1.8\,\mathrm{MA\,cm^{-2}}$, however the vortex system defrosted sooner ($j \sim 2.3\,\mathrm{MA\,cm^{-2}}$). As a result, a less strained sample showed a smaller j_c than the more strained one. Considering that such peculiarities have been observed for three different values of n_d at approximately the same values of N_c, this leads to a conclusion that it is the distribution of cracks that causes such vortex behavior. At certain values of current density and particular crack distributions, metastable states may occur when the vortices find it beneficial to stay put rather than to move towards the sample center. The frozen vortices repel their neighbors, so the penetration of new vortices into the sample becomes difficult, and the overall movement freezes. Then, as the current density increases, the Lorentz force becomes ever stronger and, at some point, it starts to prevail over vortex–vortex repulsion, so the system comes to motion again. It should be noted that the effect of vortex freezing has been observed for ($30 \leqslant N_\mathrm{c} \leqslant 420$), i.e. the range in which the obtained calculation results are qualitatively supported by experiments as has been shown in section 2.

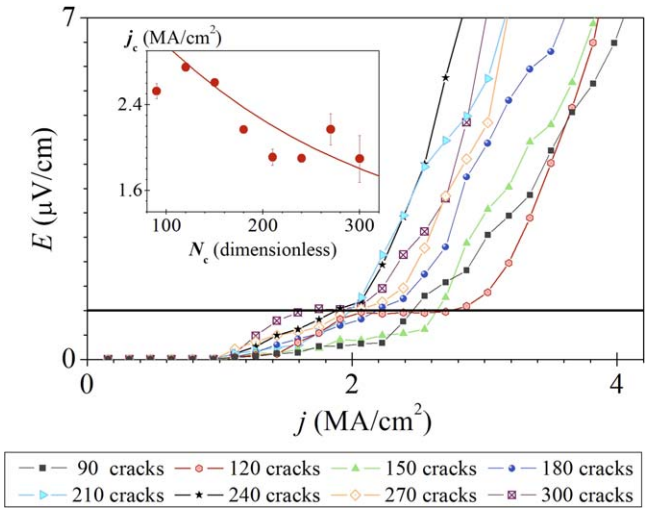

Figure 9. The *E–J* curves of samples with point defect density of 4×10^{10} cm^{-2} and different numbers of cracks from 90 to 300. The calculated points are joined directly for better perception. The insert shows a zoomed-in part of $j_c(N_c)$ dependence for a sample with $n_d = 4 \times 10^{10}$ cm^{-2} from figure 3.

4. Conclusion

In this paper, numerical Monte Carlo simulations have been carried out to study the influence of strain on the dynamics of the vortex system, the critical current density and the slope of *E–J* curves of an HTSC material. The degree of strain was modeled by adding certain areas of stress referred to as 'cracks' to the sample in a similar way they occur in a bent material in experiments.

A series of *E–J* curves have been calculated for three samples with different point defect concentrations at different degrees of strain. Each voltage–current characteristic was fitted with a power law and the exponent n (n-value) was determined. Decaying critical current density and n-value dependences on the number of cracks have been found to be in a qualitative agreement with the experiment. The limit of applicability of the calculation model has been determined.

For the first time, the staircase *E–J* curves have been observed for strained samples to correspond to the alternating freezing and defreezing of vortices. The frozen state corresponds to almost full stop of the movement of vortices which causes marginal increase in the generated electric field with the increasing current density. This phenomenon has been demonstrated on the averaged vortex configurations at different degrees of strain and in different points of the *E–J* curves. It has been shown that the occurrence of cracks creates additional channels for the vortex movement which leads to degradation of the critical current density.

Acknowledgments

This work is supported by the Russian Science Foundation under grant 17-19-01527.

The authors would like to thank Alexey I Podlivayev for help with the statement of the model and discussion of results.

ORCID iDs

Anna N Moroz https://orcid.org/0000-0003-0854-1015

References

[1] Shin H S, Kim K H, Dizon J R C, Kim T Y, Ko R K and Oh S S 2005 The strain effect on critical current in YBCO coated conductors with different stabilizing layers *Supercond. Sci. Technol.* **18** S364–8

[2] Sugano M, Machiya S, Sato M, Koganezawa T, Shikimachi K, Hirano N and Nagaya S 2011 Bending strain analysis considering a shift of the neutral axis for YBCO coated conductors with and without a Cu stabilizing layer *Supercond. Sci. Technol.* **24** 075019

[3] Sutoh Y, Kakimoto K, Kaneko N, Iijima Y and Saitoh T 2005 Mechanical bending property of YBCO coated conductor by IBAD/PLD *Physica* C **426–431** 933–7

[4] Park C, Norton D P, Budai J D, Christen D K, Verebelyi D and Feenstra R 1998 Bend strain tolerance of critical currents for $YBa_2Cu_3O_7$ films deposited on rolled-textured (001)Ni *Appl. Phys. Lett.* **73** 1904–6

[5] Cheggour N, Ekin J W, Thieme C L H, Xie Y-Y, Selvamanickam V and Feenstra R 2005 Reversible axial-strain effect in Y–Ba–Cu–O coated conductors *Supercond. Sci. Technol.* **18** S319–24

[6] Rudnev I, Mareeva A, Mineev N, Pokrovskiy S and Sotnikova A 2014 Contactless measurements of local transport characteristics of coated conductors under the bending strain *J. Phys.: Conf. Ser.* **507** 022029

[7] Shin H S and Katagiri K 2003 Critical current degradation behaviour in Bi-2223 superconducting tapes under bending and torsion strains *Supercond. Sci. Technol.* **16** 1012–8

[8] Zhang G M, Schwartz J, Sastry P V P S S, Lin L Z, Xiao L Y and Yu Y J 2004 The effects of bending strain on the critical current and AC loss of BSCCO/Ag tapes *Supercond. Sci. Technol.* **17** 1018–21

[9] Hojo M, Matsuoka T, Nakaoka S, Tanaka M, Ochiai S, Sugano M and Osamura K 2003 Bending deformation and its influence on critical current in Bi2223 composite superconducting tapes *Physica* C **392–396** 1156–61

[10] Ochiai S, Matsuoka T, Shin J K, Okuda H, Sugano M, Hojo M and Osamura K 2007 Modeling analysis of the critical current of bent Bi2223 composite tape based on the damage strain parameter and the shape of the core *Supercond. Sci. Technol.* **20** 1076–83

[11] Sugano M and Osamura K 2004 Stress–strain behavior and degradation of critical current of Bi2223 composite tapes *Physica* C **402** 341–6

[12] Katagiri K, Shin H S, Kasaba K, Tsukinokizawa T, Hiroi K, Kuroda T, Itoh K and Wada H 2003 Local variations in the critical current degradation of Ag/Bi2223 tape by tensile and bending strains *Supercond. Sci. Technol.* **16** 995–9

[13] Pan A V, Pisarenko S V and Dou S X 2009 Quantitative description of critical current density in YBCO films and multilayers *IEEE Trans. Appl. Supercond.* **19** 3391–4

[14] Pan V, Cherpak Y, Komashko V, Pozigun S, Tretiatchenko C, Semenov A, Pashitskii E and Pan A V 2006 Supercurrent transport in $YBa_2Cu_3O_{7-\delta}$ epitaxial thin films in a dc magnetic field *Phys. Rev.* B **73** 054508

[15] Golovchanskiy I A, Pan A V, Shcherbakova O V, Fedoseev S A and Dou S X 2011 An all-field-range description of the critical current density in superconducting YBCO films *Supercond. Sci. Technol.* **24** 105020

[16] Zyubin M V, Rudnev I A and Kashurnikov V A 2003 Ordered states and structural transitions in a system of Abrikosov vortices with periodic pinning *J. Exp. Theor. Phys.* **96** 1065–77

[17] Kashurnikov V A, Rudnev I A and Zyubin M V 2002 Magnetization of two-dimensional superconductors with defects *J. Exp. Theor. Phys.* **94** 377–86

[18] Kashurnikov V A, Rudnev I A and Zyubin M V 2001 Magnetization of layered high-temperature superconductors with defects: Monte Carlo simulation *Supercond. Sci. Technol.* **14** 695–8

[19] Kashurnikov V A, Maksimova A N and Rudnev I A 2013 Magnetization reversal processes in layered high-temperature superconductors with ferromagnetic impurities *Phys. Solid State* **56** 894–911

[20] Kashurnikov V A, Maksimova A N, Rudnev I A and Odintsov D S 2016 The critical current density in the layered superconductors with ferromagnetic nanorods *Physica* C **528** 17–22

[21] Kashurnikov V A, Rudnev I A, Gracheva M E and Nikitenko O A 2000 Phase transitions in a two-dimensional vortex system with defects: Monte Carlo simulation *J. Exp. Theor. Phys.* **90** 173–82

[22] Rudnev I A, Odintsov D S and Kashurnikov V A 2008 Critical current suppression in high-T_c superconductors and its dependence on the defects concentration *Phys. Lett.* A **372** 3934–6

[23] Odintsov D S, Rudnev I A and Kashurnikov V A 2006 Vortex system dynamics and energy losses in a current-carrying 2D superconducting wafer *J. Exp. Theor. Phys.* **103** 66–76

[24] Ryu S, Doniach S, Deutscher G and Kapitulnik A 1992 Monte Carlo simulation of flux lattice melting in a model high-T_c superconductor *Phys. Rev. Lett.* **68** 710–3

[25] Cheggour N, Lu X F, Holesinger T G, Stauffer T C, Jiang J and Goodrich L F 2012 Reversible effect of strain on transport critical current in $Bi_2Sr_2CaCu_2O_{8+x}$ superconducting wires: a modified descriptive strain model *Supercond. Sci. Technol.* **25** 015001

[26] Wesche R, Fuchs A M, Jakob B and Pasztor G 1995 Axial and bending strain effects in Ag and AgNiMg/Bi-2212 wires *Cryogenics* **36** 419–26

[27] Parizh M, Lvovsky Y and Sumption M 2017 Conductors for commercial MRI magnets beyond NbTi: requirements and challenges *Supercond. Sci. Technol.* **30** 014007

[28] Chudy M, Zhong Z, Eisterer M and Coombs T 2015 *n*-Values of commercial YBCO tapes before and after irradiation by fast neutrons *Supercond. Sci. Technol.* **28** 035008

[29] Kar S, Kulkarni S, Dixit M, Singh K P, Gupta A, Balasubramanyam P V, Sarangi S K and Rao V V 2012 Selection criteria of high rmT_{rmc} superconducting tapes for superconducting fault current limiter applications *IEEE Trans. Appl. Supercond.* **22** 5602804

[30] Nakayama Y, Takase N, Tagomori M, Kiuchi M and Matsushita T 1998 Effect of distribution of flux pinning strength on irreversibility line and transition line *Advances in Superconductivity X: Proceedings of the 10th International Symposium on Superconductivity* ed K Osamura and I Hibarayashi (Tokyo: Springer) p 509

[31] Anderson P W 1962 Theory of flux creep in hard superconductors *Phys. Rev. Lett.* **9** 309–11

[32] Golovchanskiy I A, Pan A V, Shcherbakova O V and Fedoseev S A 2013 Rectifying differences in transport, dynamic, and quasi-equilibrium measurements of critical current density *J. Appl. Phys.* **114** 163910

[33] Pan A V, Golovchanskiy I A and Fedoseev S A 2013 Critical current density: measurements versus reality *Europhys. Lett.* **103** 17006

[34] Pan A V, Ciovacco F, Esquinazi P and Lorenz M 1999 Depinning of a driven vortex lattice in high-T_c films *Phys. Rev.* B **60** 4293